Received: 3 July 2023 | Revised: 17 August 2023 | Accepted: 5 September 2023

DOI: 10.1002/mp.16755

RESEARCH ARTICLE

MEDICAL PHYSICS

Quantitative hemodynamic assessment of stenotic below-the-knee arteries using spatio-temporal bolus tracking on 4D-CT angiography

Pieter Thomas Boonen[1,2,3] | **Nico Buls**[1] | **Gert van Gompel**[1] | **Hannes Devos**[1] | **Yannick de Brucker**[1] | **Tim Leiner**[4] | **Dimitri Aerden**[5] | **Johan de Mey**[1] | **Jef Vandemeulebroucke**[2,3]

[1]Department of Radiology, Vrije Universiteit Brussel (VUB), Jette, Brussels, Belgium

[2]Department of Electronics and Informatics (ETRO), Vrije Universiteit Brussel (VUB), Elsene, Brussels, Belgium

[3]imec, Leuven, Belgium

[4]Department of Radiology, Mayo Clinic, Rochester, Minnesota, USA

[5]Department of Vascular Surgery, Vrije Universiteit Brussel (VUB), Jette, Brussels, Belgium

Correspondence
Pieter Thomas Boonen, Department of Radiology, Vrije Universiteit Brussel (VUB), Laarbeeklaan 101, 1090 Jette, Brussels, Belgium.
Email: Pieter.thomas.boonen@vub.be

Funding information
Fonds Wetenschappelijk Onderzoek, Grant/Award Number: 1S63719N

Abstract

Background: Peripheral arterial disease (PAD) is a chronic occlusive disease that restricts blood flow in the lower limbs, causing partial or complete blockages of the blood flow. While digital subtraction angiography (DSA) has traditionally been the preferred method for assessing blood flow in the lower limbs, advancements in wide beam Computed Tomography (CT), allowing successive acquisition at high frame rate, might enable hemodynamic measurements.

Purpose: To quantify the arterial blood flow in stenotic below-the-knee (BTK) arteries. To this end, we propose a novel method for contrast bolus tracking and assessment of quantitative hemodynamic parameters in stenotic arteries using 4D-CT.

Methods: Fifty patients with suspected PAD underwent 4D-CT angiography in addition to the clinical run-off computed tomography angiography (CTA). From these dynamic acquisitions, the BTK arteries were segmented and the region of maximum blood flow was extracted. Time attenuation curves (TAC) were estimated using 2D spatio-temporal B-spline regression, enforcing both spatial and temporal smoothness. From these curves, quantitative hemodynamic parameters, describing the shape of the propagating contrast bolus were automatically extracted. We evaluated the robustness of the proposed TAC fitting method with respect to interphase delay and imaging noise and compared it to commonly used approaches. Finally, to illustrate the potential value of 4D-CT, we assessed the correlation between the obtained hemodynamic parameters and the presence of PAD.

Results: 280 out of 292 arteries were successfully segmented, with failures mainly due to a delayed contrast arrival. The proposed method led to physiologically plausible hemodynamic parameters and was significantly more robust compared to 1D temporal regression. A significant correlation between the presence of proximal stenoses and several hemodynamic parameters was found.

Conclusions: The proposed method based on spatio-temporal bolus tracking was shown to lead to stable and physiologically plausible estimation of quantitative hemodynamic parameters, even in the case of stenotic arteries. These parameters may provide valuable information in the evaluation of PAD and contribute to its diagnosis.

KEYWORDS
4D-CT, B-spline regression, contrast bolus tracking, hemodynamics, image processing, peripheral arterial disease, spatio-temporal

1 | INTRODUCTION

1.1 | Clinical context

Lower extremity peripheral arterial disease (PAD) is a chronic atherosclerotic occlusive disease that causes a reduced blood flow towards the lower extremities due to partial or complete obstruction of one or more peripheral arteries.[1,2] It is the third leading cause of atherosclerotic vascular morbidity after coronary heart disease and stroke,[3] and is associated with an elevated mortality risk and significantly impaired quality of life.[4] The European prevalence is estimated at 7.99 %.[5] If the arterial flow further decreases, PAD degenerates into critical limb ischemia, which is associated with high mortality, amputation and irreversible damage to the leg.[6] A detailed diagnosis of lower extremity PAD is therefore vital to prevent further development and to devise an optimal revascularization strategy.

Severity of occlusive disease in the lower extremities is determined by the aggregate assessment of flow-limiting lesions, hence by taking into account location and extent of the stenosis. Digital subtraction angiography (DSA) has long been considered the gold standard for evaluating PAD but has been replaced by computed tomography angiography (CTA) and contrast-enhanced magnetic resonance angiography (CE-MRA).[7–9] Both run-off CE-MRA and run-off CTA are reliable non-invasive imaging modalities, providing a high accuracy and sensitivity for detecting stenoses in arterial segments from the aorta up to the popliteal artery.[10,11]

In run-off CTA, a helical acquisition from the diaphragm to the toes is acquired with intravenous contrast injection. A failure rate of 7.3% in providing an acceptable diagnosis has been reported in the below-the-knee (BTK) arteries.[9] This is due to multiple reasons: (i) delayed contrast bolus with respect to the CT acquisition caused by proximal hemodynamically significant lesions[12] or patient-to-patient variations[13]; (ii) limited spatial resolution to assess the residual lumen of the BTK arteries (1–3 mm); (iii) presence of vessel wall calcifications, often encountered in patients with diabetes or renal failure, causes artifacts which severely hampers the assessment of lesion morphology as it is difficult to differentiate between calcifications and contrast agent.[14] In addition, the run-off CTA does not allow for a detailed assessment of the effect of hemodynamic significant lesions on the arterial blood flow. The added benefit of flow measurements has however been extensively examined in other, larger, arterial beds.[15–18] Likewise, venous enhancement, motion artefacts, and signal loss caused by severe calcifications or stainless steel stents/implants might reduce the image quality and diagnostic accuracy of run-off CE-MRA. Additionally, achieving the high spatial resolution needed for assessing the BTK arteries requires longer acquisition times or even a dedicated acquisition with a separate injection of contrast agent.

To overcome these limitations, there is a growing interest in adding dynamic series to the static, single phase acquisition of BTK arteries using dynamic or 4D-CT acquisitions. Previous studies have reported an improved diagnostic accuracy for dynamic CTA.[19,20] However, these studies focused exclusively on qualitative results of dynamic imaging, that is, the improved assessment of lesion morphology and degree of stenosis.

1.2 | Hemodynamic assessment

A sequence of dynamic CT acquisitions at timed intervals allows one to track the injected contrast bolus propagating through the arterial conduit. A time attenuation curve (TAC), also called time density curve or arterial input function (AIF)-the latter in the context of tissue perfusion analysis- represents the local changes in intensity over time, caused by the temporal passages of the iodine contrast bolus. Reliably measuring the TAC is essential to access the quantitative (hemodynamic) parameters required to analyse the blood flow circulation in the BTK arteries.[21] These descriptive parameters can however be affected by the instability of the curves due to the presence of imaging noise and artefacts, or due patient motion across the image sequence. If the interval between two subsequent acquisitions, that is, interphase delay, is too large, the propagating contrast bolus can be partially or completely missed. In addition, small vessel diameter and partial volume effect further hamper the reliability of the TAC measurement. Estimating the TAC and the parameters derived from the TAC, is therefore highly challenging. Previous attempts to assess the TAC have been made by several authors (Table 1). Whereas their research is mainly focused on assessing the AIF in order to quantify (cerebral) perfusion, the algorithms could be applicable for assessing the TAC in the BTK arteries.

Cheong *et al.*[22] introduced two piecewise continuous regression models to quantify the bolus arrival time (BAT) using Monte Carlo simulation experiments, respectively a linear-linear model and a linear-quadratic model. Although both models were successful in accurately assessing the BAT, it was noted by the authors

TABLE 1 Overview of the related work regarding bolus tracking and fitting of the time attenuation curves.

Reference	Anatomy	Algorithm
Cheong *et al.*[22]	Generic: Monte Carlo simulations	Linear-linear, linear-quadratic
Bennink *et al.*[23]	Cerebral arteries	Gamma variate
Barfett *et al.*[18]	Internal carotid & cerebral arteries	Gamma variate, Gaussian, quadratic
Kasasbeh *et al.*[24]	Cerebral arteries	Gamma variate
Giacalone *et al.*[26]	Numeric simulations	Spatio-temporal deconvolution
Boonen *et al.*[29]	BTK arteries	Quadratic
Bendinger *et al.*[27]	Simulations & rats	1D smoothing splines
Peerlings *et al.*[25]	Cerebral arteries	Gamma variate
Chakwizira *et al.*[28]	Simulations & cerebral arteries	1D cubic Bézier curves
Proposed	*Below-the-knee arteries*	*2D Spatio-temporal B-spline*

Abbreviation: TAC, time attenuation curves.

that their performance could deteriorate for broad TAC's. Barfett *et al.*[18] estimated the TAC with three different functions (gamma variate function, Gaussian function and local quadratic function) in order to assess the time to peak (TTP) and flow velocity along a vessel centroid, defined via mouse clicks, in different setups. The Gaussian curve fitting produced the best result in a simulated flow channel whereas the quadratic function provided the best fit in the flow phantom experiment. The authors reached no conclusion regarding the in vivo studies. For stroke imaging, multiple authors[23–25] used a gamma variate function to accurately fit the TAC and to assess the mean blood volume (MBV), TTP, cerebral blood flow (CBF), mean transit time (MTT), BAT, area under the curve (AUC) and the amplitude. Whereas most authors focus mainly on temporal regularization of the TAC, Giacalone *et al.*[26] introduced a deconvolution algorithm based on both temporal and edge preserving spatial regularization in the context of ischemic stroke using a numeric simulator. The authors suggested that spatial organization of ischemic tissue in the brain should be taken into account, contrarily to the solely temporal regularization approach in which each voxel is processed independently. The proposed spatio-temporal model outperformed temporal algorithms. Bendinger *et al.*[27] proposed an approximation of the TAC by a smoothing spline and estimated the parameters using generalized cross validation based on the ratio of the mean squared error and the degrees of freedom. The proposed method was deemed suitable for accurate BAT estimation. Chakwizira *et al.*[28] evaluated the feasibility of applying a deconvolution method based on 1D cubic bézier curves for perfusion quantification in cerebral dynamic MRI using both simulated data and one healthy volunteer. The cubic Bézier curves, implemented in a Bayesian framework, provided accurate perfusion estimates and smooth residue functions. Higher-order curves did not improve the results while elevating the computational cost.

We previously tested the feasibility of blood velocity quantification in BTK arteries using 4D-CTA in six patients with clinical suspicion of PAD.[29] We were able to track the propagation of the contrast bolus through the arteries and we assessed the TTP and the average blood flow velocity by fitting a 2nd degree polynomial to the TAC. No significant correlation between the assessed parameters and the presence of stenoses was found.

The current study seeks to quantify the arterial blood flow in the BTK arteries in patients with PAD. Three primary aims are envisaged: (i) to segment the BTK arteries; (ii) to create a robust TAC fitting method; (iii) to estimate quantitative hemodynamic parameters with high precision and to examine how they are affected by PAD. To this end, we propose a novel method based on bicubic B-spline surface fitting to assess the blood flow in patients suffering from PAD using 4D-CTA, taking into account the spatio-temporal nature of the data.

2 | MATERIALS AND METHODS

Ethical approval for this retrospective study was obtained from the institutional review board, Ethics Committee (UZ Brussel, BUN 1432023000074). We selected patients with suspected PAD which were referred for standard run-off CTA and 4D-CT.

2.1 | 4D-CT image acquisitions

Patients underwent two subsequent CT acquisitions: (1) A standard run-off CTA used for clinical diagnosis and (2) an additional diagnostic 4D-CT examination at the level of the calves. All scans were performed on a 256-slice wide beam CT (Revolution CT, GE Healthcare, 100 kV, auto mA) and patients were placed on the table in a supine, feet-first position.

The run-off CTA was performed with a helical acquisition from above the diaphragm towards the toes with the following scan parameters: 40 mm (64 × 0.625) collimation, 39.4/s mm table feed, 0.98 pitch and 0.5 s tube rotation. 55 mL iodine contrast agent (370 mg I/mL, Ultravist, Bayer Healthcare) was injected intravenously at a rate of 5.0 mL/s, followed by 35 mL at 3.0 mL/s and a 40 mL saline flush at 3.0 mL/s. The run-off CTA was triggered when the bolus tracker positioned on the aorta reached a CT value of 125 HU.

After a 10 min delay, the 4D-CT data were acquired by performing 18 repeated axial acquisitions on the distal half of the tibia at a 2 s interphase delay with 160 mm (256 × 0.625 mm) collimation and 0.5 s tube

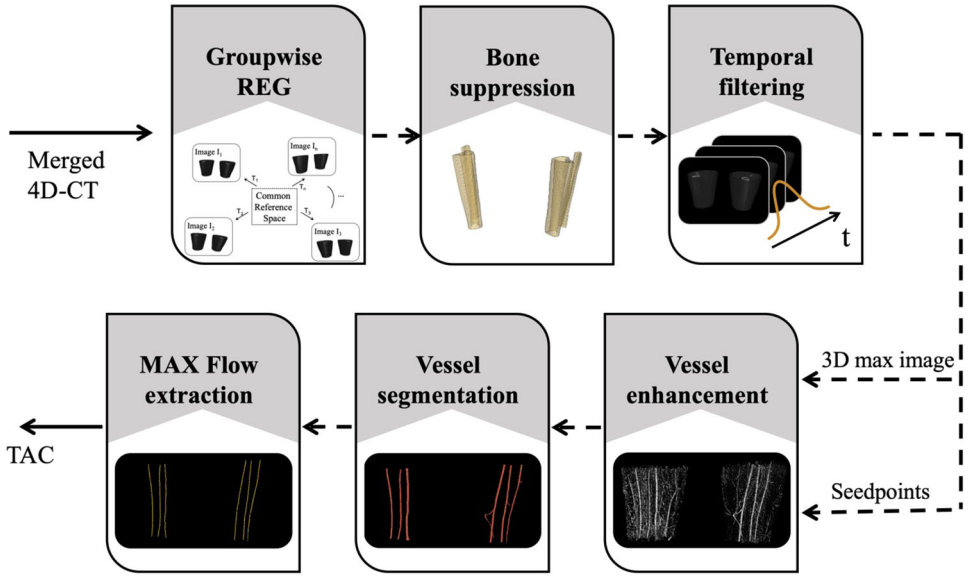

FIGURE 1 Proposed workflow for the automated segmentation of the BTK arteries from 4D-CT imaging. BTK, below-the-knee; CT, Computed Tomography.

rotation. Incorporating the 2 s interphase delay allowed longer total scanning times (34 s) without increasing the number of acquisitions. This way, the patient dose was reduced, but the acquisitions were still obtained sufficiently fast to capture the passing contrast bolus and assess the blood flow rate. A biphasic injection protocol was used to administer 35 mL of iodine contrast agent at a rate of 5.0 mL/s, followed by 15 mL at 3.0 mL/s and a 40 mL saline flush at 3.0 mL/s. The first acquisition started 20 s after contrast injection. The effective dose for the run-off CTA and the 4D-CT series were respectively 5.1 mSv and 0.2 mSv (ICRP-103 guidelines).[30]

2.2 | Arterial segmentation

All patient data were de-identified and the CT images were transferred to an offline workstation. In-house developed software, written in Python and C++ based on the Insight Segmentation and Registration Toolkit (ITK),[31] was used for processing the images.

The following pipeline was considered to segment the BTK arteries (Figure 1). This pipeline was created and fine-tuned based on five arteries which were manually selected to depict different grades of stenoses and different arterial structures such as branches.

2.2.1 | Motion correction

To mitigate the effect of unwanted patient movement during the 4D-CT acquisitions, a groupwise,[32] non-rigid registration approach based on B-splines was used in the first step. For each patient, all 18 temporal sequences were simultaneously registered to common reference space, taking into account the information of all the images during the process without having a bias towards a manually selected reference image. As metric, the variance over last dimension metric was applied as suggested by Metz *et al.*[33] for groupwise registration. For the optimization process, the adaptive stochastic gradient descent optimizer was used with 2000 samples, randomly selected in every iteration, and run for 2000 iterations.

2.2.2 | Vessel segmentation

Secondly, a mask of bones and potential calcifications was created and extracted from the registered 4D image to facilitate segmentation of the arteries. To ensure no iodine contrast was included in this mask, the minimum intensity over the temporal domain was first calculated for each voxel, eliminating the propagating iodine contrast. The mask was then obtained from this 3D minimum intensity image by applying Otsu thresholding, mathematical morphology (opening) and connected component analysis, keeping the four largest components. After removing bones and potential calcifications from the 4D registration data set, a recursive Gaussian filter[34] was applied over the temporal dimension to reduce image noise along the time axis while maintaining spatial resolution to aid the segmentation process. A standard deviation of 1 s was found to smooth the passing contrast bolus sufficiently.

Next, to enhance the arteries, the vesselness filtering algorithm was employed using the vascular modeling

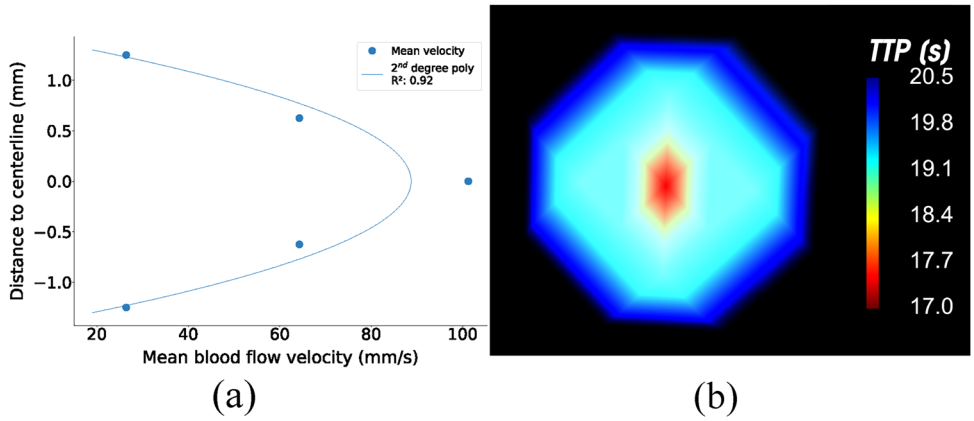

FIGURE 2 (a) Parabolic velocity profile fitted over the mean blood flow velocities as a function of distance from the arterial centerline in an artery. (b) Example of an arterial cross-section visualizing the TTP (s) by means of color-coding: early arrival is depicted in red, late in blue. TTP, time to peak.

toolkit (VMTK[35]). This vessel enhancement filter, based on Frangi's method,[36] highlights tubular vessel structures on the basis of eigenvalues of the Hessian matrix while suppressing other shapes such as plates and blobs. This particular vesselness filter requires an 3D image as input and an optional list of seed points. As input image, the maximum intensity projection (MIP) of each voxel over the temporal domain was used. The seed points were obtained by computing the local variance over time in each voxel, followed by a rough artery segmentation using Otsu thresholding.

Finally, the BTK arteries, that is, anterior tibial artery (ATA), peroneal artery (PL) and posterior tibial artery (PTA), were segmented from the enhanced vessel image applying a threshold of 0.1 (normalized) Hounsfield Units (HU) and using connected component analysis to segment the three largest vessels in each leg and provide them with an unique label. The segmented arteries were visually checked afterwards to validate the segmentation method and to verify if the label matched with the corresponding artery name.

2.2.3 | Extraction of maximum blood flow in the arteries

Figure 2a shows an example of the quantified mean blood flow velocity over the entire length of the segmented artery as a function of the distance to the centerline. The measurements illustrate the characteristics of a fully developed laminar flow in the BTK arteries, and show fair agreement with the parabolic velocity profile ($R^2 = 0.92$) as described by Poiseuille's law.[37] Due to wall shear stress, the mean blood flow velocity is highest in the center of the artery and decreases towards the arterial wall. This effect also impacts other hemodynamic parameters, as illustrated for TTP assessment (Figure 2b). For this example, pixel-wise computation of TTP over the cross-section revealed that the contrast arrived up to 3 s earlier at the centerline the artery compared to one and two pixels distance from the center.

The previous example illustrates that averaging intensities or hemodynamic parameters over the entire cross-section may reduce the observed dynamics in the observed TAC's. To minimize this effect, we only include intensities from a smaller sub region of interest to extract TAC's as opposed to including the complete artery. A morphological centerline segmentation however is sensitive to errors and may not correspond to the sub region representing substantial blood flow in stenotic patients. Therefore, we identified the hemodynamically dominant sub region where the passage of the bolus is most apparent. A cross-shaped structuring element was moved across each axial cross-section of the segmented artery (*xy*-plane) and it's position was set to that for which the pixels yielded the highest median variance in intensity over time.

2.3 | Blood flow assessment

In order to assess blood flow in BTK arteries, we first obtained the TAC's in each arterial voxel. Then, we assessed its descriptive parameters to characterize and quantify the arterial blood flow in the BTK arteries.

2.3.1 | TAC fitting

TAC curve fitting in the context of BTK arteries is highly challenging. Arteries are small and suffer from partial volume effect. At acceptable imaging dose, measurements are noisy and further hampered by patient motion or imperfect alignment after registration. To maximally exploit the acquired data and improve robustness, we propose a global, spatio-temporal regression approach, enforcing both temporal (evolution of the bolus at location of the artery over time) and spatial smoothness

(shape of the bolus over the imaged artery at a given time). To this end we implemented a non-parametric regression approach based on uniform 2D B-splines.[38] Approximation B-splines of degree two or higher allow to estimate continuous and smooth functions, their extension to higher dimensions is straightforward and allow to control the degrees of freedom per dimension. The used formulation of the 2D B-spline surface is given as follows:

$$S(t,x) = \sum_{i=0}^{m}\sum_{j=0}^{n} d_{i,j} N_{i,k}(t) N_{j,k}(x) \quad (1)$$

Where the B-spline surface $S(t, x)$ is generated as the tensor product of two univariate B-splines curves, $N_{i,k}(t)$ and $N_{j,k}(w)$, both of the same order (k), defined by $(m + 1) \times (n + 1)$ control points ($d_{i,j}$).

To evaluate the benefit of the spatio-temporal fitting approach, we compare it to a 1D temporal B-spline approach, inline with the commonly performed temporal fitting of a TAC. The formulation for a 1D B-spline curve of order k and $(m + 1)$ control points (d_i) was as follows:

$$P(t) = \sum_{i=0}^{m} d_i N_{i,k}(t) \quad (2)$$

Both fitting method were carried out on the original data (4D data set, after registration, without temporal smoothing) using the least-squares bivariate spline approximation of scipy.[39] All relevant parameters such as the degree of splines and the number and coordinates of the control points were determined using cross validation with a 90-10 train-test distribution and 10 folds on the complete data-set.

2.3.2 | Hemodynamic parameter assessment

From the fitted TAC's, the following parameters, commonly studied in literature,[17,21,40] were estimated: time of arrival (TOA,s), TTP(s), mean velocity (mm/s), mean blood flow rate (mL/min), slope, full width at half maximum (FWHM,s) or the transit time, peak intensity (PI, HU) and blood volume or AUC. Figure 3 shows an example TAC and its descriptive parameters. The TOA and the TTP correspond to the time required for a voxel to attain 30% of its maximum intensity[41] and the time required for a voxel to reach its maximum intensity, respectively. These parameters measure the extent of delay in contrast arrival time, which is expected to be relatively consistent across all BTK arteries. The mean blood flow velocity was computed fitting a linear regression to the TTP values as a function of distance along the artery (mm). The enhancement slope is an indication for the contrast intake in the assessed region

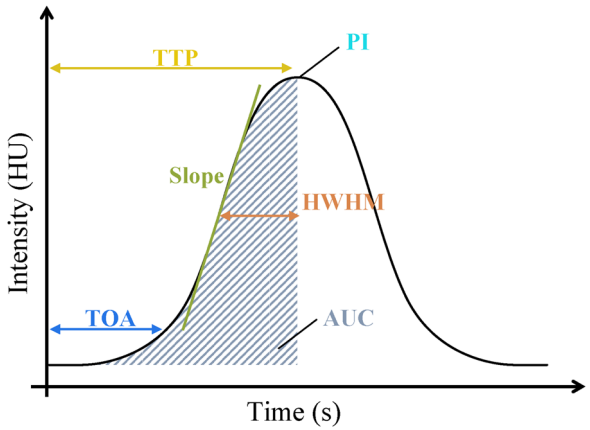

FIGURE 3 A TAC and all descriptive parameters which are assessed from the curve: TOA, (s), TTP,(s), slope, HWHM, (s), peak intensity (PI, HU) and AUC. AUC, area under the curve; HU, Hounsfield Units; HWHM, half width at half maximum; PI, peak intensity; TAC, time attenuation curve; TOA, time of arrival; TTP, time to peak.

and corresponds to the rising slope of the TAC. In the case of heavily occluded proximal arteries, the second half of the TAC, that is, the contrast washout, could not always be obtained due to the delayed contrast propagation. Therefore, the half width at half maximum (HWHM,s) was obtained from the TAC's instead of the FWHM. Similarly, we limited the AUC to the first part of the TAC and implemented it from sklearn.[42] In order to determine the mean volumetric blood flow rate (mL/min), the average blood velocity was measured throughout the entire artery, rather than solely focusing on the hemodynamically dominant sub-region. Subsequently, the obtained mean velocity was divided by the average cross-sectional area of the artery, which was determined from the arterial segmentations.

2.3.3 | Reproducibility of hemodynamic parameter assessment

As indicated before, the hemodynamic assessment is highly challenging for several reasons, including, relatively low temporal sampling, small arterial cross-sections and the fact the contrast bolus is no longer sharply delineated at the level of the calves, in particular in the case of pathological arteries. To demonstrate the robustness of the proposed pipeline, the reproducibility of hemodynamic assessment with respect to interphase delay and imaging noise was evaluated. To this end, a subset was created by removing half of the original time-points (nine temporal phases instead of 18), causing the interphase delay to increase from 2 to 4 s. Additionally, five subsets were created by adding Gaussian noise of mean zero and increasing sigma value from 0 to 100 HU in steps of 20 HU.

Hemodynamic parameter estimation was performed on these deteriorated data sets and the results were compared with the results of the original data-set using Bland-Altman plots. The comparison was also performed in case of 1D temporal fitting, to evaluate the benefit of the spatio-temporal approach.

2.4 | Clinical application

In order to demonstrate the potential of the hemodynamic assessment in diagnosing PAD, we provided a detailed description of a single patient's case. We conducted an analysis that involved comparing two hemodynamic parameters (TTP and flow rate) with the results of the clinical run-off CTA, thereby establishing a correlation between these parameters and the severity of PAD. Furthermore, we examined the impact of hemodynamically significant lesions on the blood flow in the BTK arteries across multiple patients. To this end, two board certified radiologists (H.D. and Y.d.B., 14 years of experience) independently reviewed the run-off CTA and 4D-CTA and assessed all arterial segments distal from the aorta-bifurcation. In case of inconsistent assessments, a final consensus was obtained. Occlusive disease in each segment was graded based on the most flow-limiting lesion using a three-point confidence scale proposed by Sommer *et al.*[43]: 0=no significant stenosis (<50%), 1=significant stenosis (50–99%) and 2=complete occlusion (100%). For each of the BTK arteries, the scores of all proximal segments were added up with the score of the respective BTK artery. Based on these scores, two classes were created to differentiate between non stenotic/occluded arteries (sum=0) and stenotic/occluded arteries (sum≥1). Differences in parameter values between both classes were evaluated using the Mann-Whitney U test (IBM SPSS Statistics V28).

3 | RESULTS

The CT acquisitions of fifty patients (mean age 63 years old, 23 male, 26 female) were included in this study. One patient was excluded from the analysis as the contrast did not reach the BTK arteries during the 4D-CT acquisition due to severe occlusions. One patient had an absent ATA in both legs which was considered a normal anatomical variant.

3.1 | Arterial segmentation

The total amount of included BTK arteries was 292. Applying the automated segmentation pipeline, 280 were successfully segmented (96%). Severe calcifications yielded an inadequate variance in intensity values, causing the segmentation to fail for ten arteries. In one artery, the contrast bolus did not arrive during the 4D-CT acquisition. A last failure was due to a vein which was segmented together with the artery caused by a high cardiac output. The average diameter of the BTK arteries was 2.99 mm ± 0.72 mm.

3.1.1 | Extraction of maximum blood flow in the arteries

Figure 4 shows a 3D comparison of the median intensity value (HU) for each cross section as a function of distance along the artery (mm) and time (s) using the entire cross section (4a) and the extracted sub region of maximum flow (4b). From these plots, it is clear that a higher signal to noise is obtained using the hemodynamic sub region. When averaging over the entire cross section, the dynamics of the propagating contrast bolus, needed for TAC fitting, are not apparent.

3.2 | Blood flow assessment

3.2.1 | TAC fitting

Using cross validation, the TAC fitting based on bicubic B-splines yielded an optimal root mean square error and coefficient of determination (R^2) of the test data. Relatively small differences between four, five and six control points were found. To avoid over-fitting the TAC, we selected four control points, uniformly placed over the spatial- and temporal axis.

Figure 5a shows exemplary TAC's, obtained from bicubic spatio-temporal TAC fitting in a healthy artery. The 2D approach results in a smooth time attenuation surface (TAS) as opposed to the sharply delineated TAC's obtained using 1D temporal fitting (Figure 5d). The TAC distortions are more apparent in a pathological artery (Figures 5b and 5e) as the contrast bolus arrives too late and the TAC is interrupted before reaching its maximum intensity.

3.2.2 | Hemodynamic parameter assessment

Figure 5c visualizes the median TOA, TTP, slope and HWHM for each cross section as a function of time, superimposed on the 2D fitted TAC's in a stenotic artery. As can be seen from the 3D plot, the obtained hemodynamic parameters are continuous along the distance axis, with gradually increasing TOA and TTP values. The same hemodynamic parameters derived from the 1D fitted TAC's are visualised in Figure 5f. Using the 1D method, the estimation of the hemodynamic parameters proved to be more unstable, leading to scattered values.

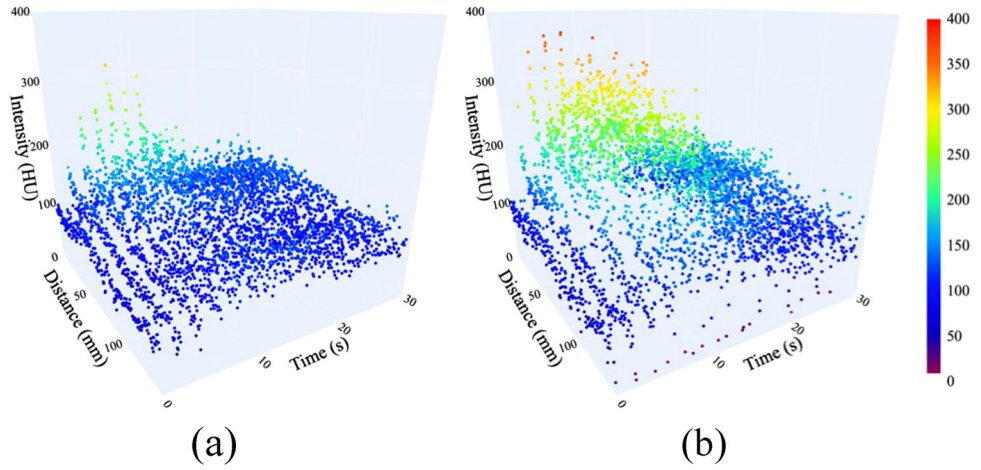

FIGURE 4 3D plot showing the original intensity signal (HU) as a function of distance along the artery (mm) and time (s) obtained using the complete arterial cross-section (a) and the region of maximum flow (b). HU, Hounsfield Units.

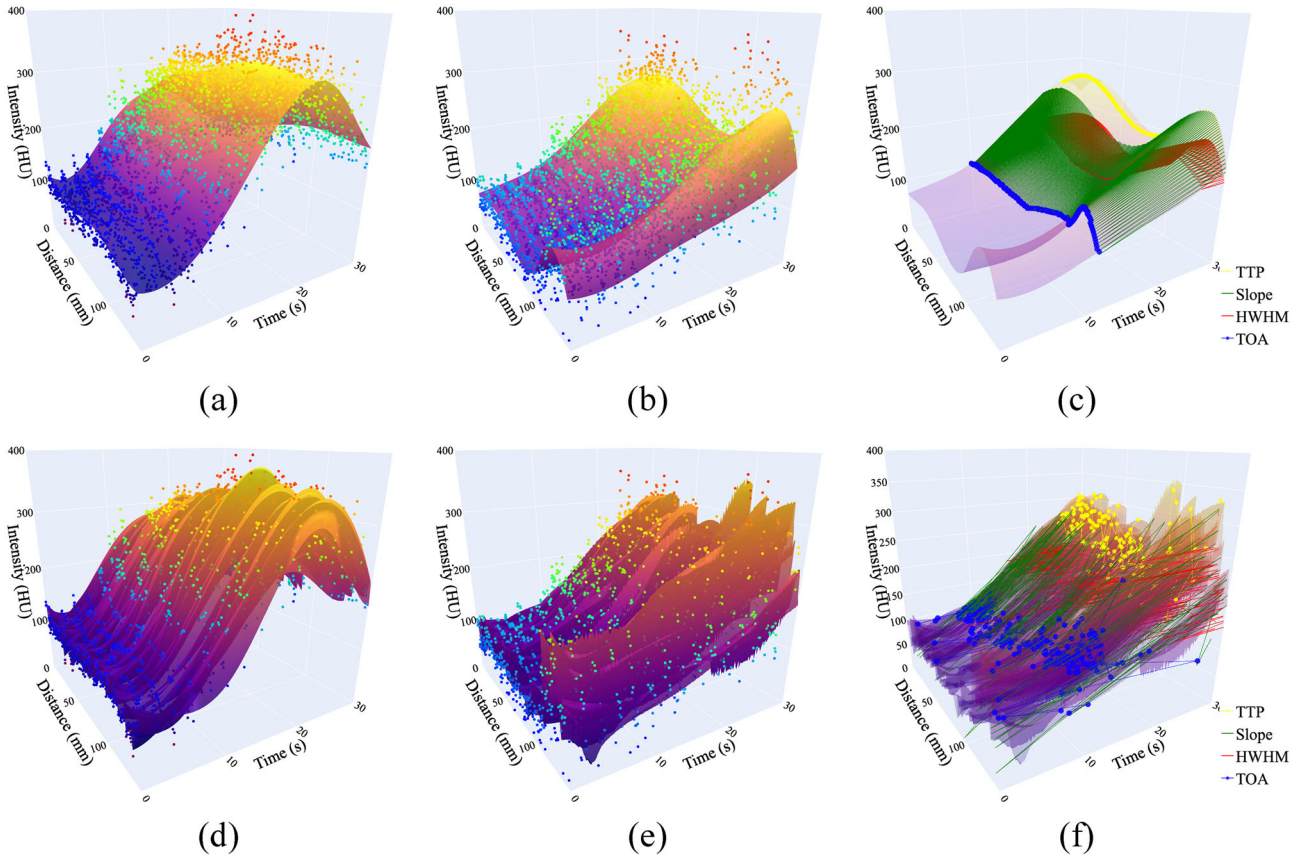

FIGURE 5 3D visualization of the original intensity signal (HU) as a function of distance along the artery (mm) and time (s) (dots) and the corresponding TAC fitting and parameter estimations. Top: results of TAC fitting using spatio-temporal 2D regression, superimposed on the original intensity signal in a healthy (a) and pathological (b) artery. (c) Visualization of the obtained TOA, TTP, slope and HWHM from the 2D fit within a pathological artery. Bottom: results of TAC fitting using temporal 1D regression, superimposed on the original intensity signal in a healthy (d) and pathological (e) artery. (f) Visualization of the obtained TOA, TTP, slope and HWHM from the 1D fit within a pathological artery. HU, Hounsfield Units; HWHM, half width at half maximum; TAC, time attenuation curve; TOA, time of arrival; TTP, time to peak.

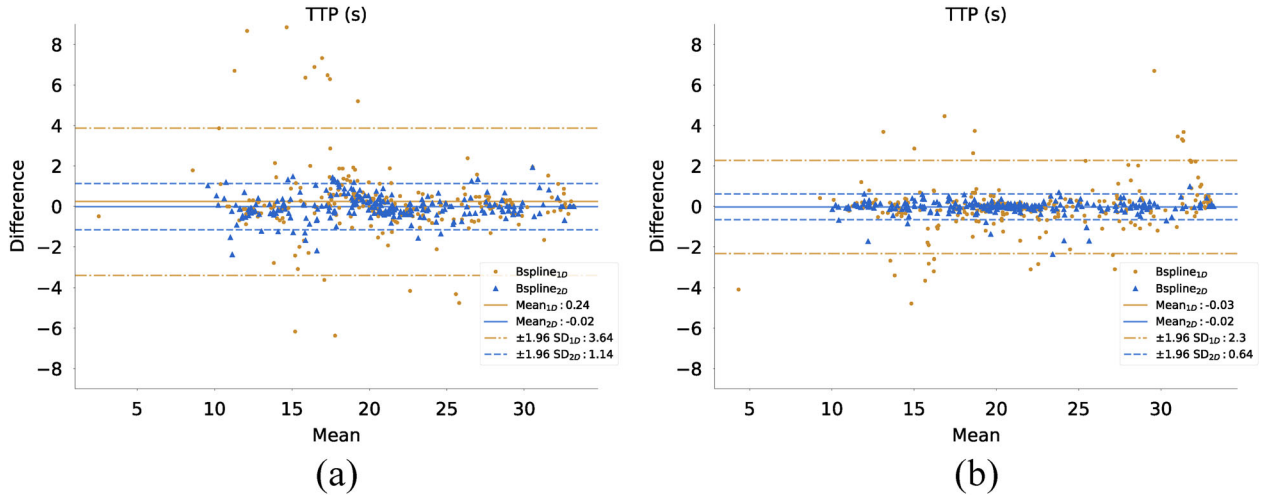

FIGURE 6 Bland Altman plots to analyse the reproducibility of 1D temporal TAC fitting (orange) and 2D spatio-temporal TAC fitting (blue). (a) comparison of fitted TAC's between the original data (Δt = 2s) and temporal subset (Δt = 4s) for TTP. (b) Comparison between the original data and the subsets with increased Gaussian noise (σ = 20, 40, 60, 80, 100) visualized for TTP. TAC, time attenuation curve; TTP, time to peak.

3.2.3 | Reproducibility of hemodynamic parameter assessment

The Bland Altman plot in Figure 6a compares the obtained TTP values from the original data (Δt = 2s) and the temporal subset (Δt = 4s) applying the 1D temporal (orange) and 2D spatio-temporal (blue) fitting method. The comparison between the TTP values from the original data and the noisy subset (σ = 20, 40, 60, 80, 100) is represented in Figure 6b. From these plots it is apparent that both increasing the interphase delay and adding image noise results in larger standard deviations for the 1D method compared to the 2D method, indicating less precise estimations for the temporal fitting with respect to the spatio-temporal approach. The results for the other descriptive hemodynamic parameters are provided in Table 2. The 1D temporal fitting approach consistently introduced larger biases and standard deviations compared to the 2D spatio-temporal method. Increasing the interphase delay does not seem to have a large impact on the hemodynamic parameters derived from the 2D fitted TAC. Overall, the TTP proved to be the most robust hemodynamic parameter.

3.3 | Clinical application

Figure 7a shows the MIP derived from the run-off CTA, used as standard of care in PAD diagnosis to provide a complete overview of the vascular tree at a glance. The BTK arteries on both sides are opacified but the contrast gets overtaken by the gantry more distally, resulting in insufficiently delineated arteries in the left calf and foot. This patient was diagnosed with two stenoses at knee-level on the left side and one stenosis in both the left ATA and left PL. On the right side, a local stenosis was detected in the ATA. This resulted in a total grading score of 3,3,2 and 1,0,0 in respectively the left and right ATA, PL, and PTA. Figure 7b visualizes a volume rendering of the segmented BTK arteries. As a result of the proximal stenosis in the left leg, higher TTP values in the BTK arteries (21.0–25.0 s) are apparent compared to the ones on the right (19.0–21.0 s) (Figure 7c). Based on the highest mean flow rate (Figure 7d), the PTA is the dominant BTK artery on both sides. For the left leg, this corresponds to the artery with the lowest grading score, that is, two. On the right side, the dominant artery corresponds with grading score zero. In addition, there is a noticeable difference in both TPP and mean blood flow rate compared to the the stenotic artery (ATA).

Out of 292 BTK arteries, 140 were evaluated having no significant stenosis (48%) and 152 having one or more significant stenoses and/or total occlusions (52%). Table 3 provides an overview of the two grading classes (0 & 1) and their corresponding hemodynamic parameters. For all hemodynamic parameters except velocity and mean flow rate, the average values of the three most distal slices along the artery are reported. The 2D spatio-temporal TAC fitting led to physiologically plausible values regarding all hemodynamic parameters. Applying the Mann Whitney U test to test for differences between the two groups, a significant increase in TOA ($p < 0.001$) and TTP ($p < 0.001$) for the stenotic arteries can be noticed. On the other hand, a significant decrease in slope ($p = 0.006$) and PI ($p < 0.001$) can be observed. No significant difference between the non-stenotic and stenotic arteries could be found based on the mean velocity ($p = 0.276$), HWHM ($p = 0.653$) and AUC ($p = 0.434$), although showing a slight tendency towards decreasing values within stenotic arteries. Mean flow rate values ($p = 0.711$) were slightly higher in stenotic arteries compared to non-stenotic arteries.

TABLE 2 Results of the Bland Altman comparison of reproducibility for the 2D spatiotemporal TAC fitting and 1D temporal TAC fitting.

	$\sigma = 20$		$\sigma = 40$		$\sigma = 60$	
	2D	**1D**	**2D**	**1D**	**2D**	**1D**
TOA	0.08 ± 3.71	0.26 ± 4.47	0.04 ± 4.66	0.61 ± 5.02	0.14 ± 4.65	1.02 ± 6.91
TTP	0.00 ± 0.50	–0.07 ± 1.93	0.00 ± 0.67	–0.08 ± 2.59	–0.09 ± 1.26	–0.01 ± 3.24
Slope	0.03 ± 4.18	–1.42 ± 53.65	–0.26 ± 5.70	0.83 ± 8.74	–0.08 ± 7.16	1.51 ± 11.84
HWHM	–0.02 ± 0.49	–0.05 ± 2.21	0.01 ± 0.66	–0.09 ± 2.44	–0.07 ± 1.33	–0.25 ± 3.25
PI	3.31 ± 105.43	–12.89 ± 651.63	–2.85 ± 146.74	16.59 ± 174.53	0.29 ± 161.96	34.33 ± 227.08
AUC	–16.49 ± 383.16	–57.17 ± 913.96	2.13 ± 453.29	–109.78 ± 915.08	–39.54 ± 1002.22	–132.7 ± 1278.83
	$\sigma = 80$		$\sigma = 100$		**€t = 4s**	
	2D	**1D**	**2D**	**1D**	**2D**	**1D**
TOA	0.5 ± 5.08	1.43 ± 7.22	0.83 ± 7.60	1.36 ± 8.21	–0.22 ± 2.60	1.45 ± 5.97
TTP	–0.01 ± 1.00	–0.10 ± 3.73	–0.03 ± 1.96	0.01 ± 4.77	–0.02 ± 1.14	0.24 ± 0.64
Slope	0.16 ± 8.38	1.9 ± 13.68	0.39 ± 11.06	2.52 ± 15.95	–0.47 ± 6.30	3.21 ± 37.7
HWHM	–0.11 ± 2.76	–0.26 ± 4.02	–0.16 ± 2.69	–0.30 ± 4.82	0.00 ± 1.39	–0.09 ± 3.58
PI	10.59 ± 225.14	32.55 ± 317.52	9.61 ± 293.35	44.49 ± 302.26	–9.34 ± 198.68	67.62 ± 498.33
AUC	–19.36 ± 661.96	–201.91 ± 1490.97	–81.94 ± 1148.47	–196.21 ± 1614.62	15.07 ± 529.23	–126.22 ± 1265.42

Note: Mean difference ± standard deviation is given for each hemodynamic parameter between the original data set and the deteriorated data sets ($\sigma = 20,40,60,80,20$ & $\Delta t = 4$ s).
Abbreviations: AUC, area under the curve; HWHM, half width at half maximum; PI, peak intensity; TAC, time attenuation curve; TOA, time of arrival; TTP, time to peak.

TABLE 3 Assessed mean hemodynamic parameters ± the standard deviation.

Class	Velocity (mm/s)	Flow rate (mL/min)	TOA(s)	TTP(s)	Slope	HWHM (s)	PI (HU)	AUC
0	54.49 ± 67.44	16.58 ± 44.17	9.26 ± 6.56	20.55 ± 6.04	26.82 ± 10.89	6.11 ± 1.96	464.27 ± 78.02	2571.76 ± 1012.36
1	51.24 ± 49.76	18.68 ± 32.93	12.81 ± 7.83	23.74 ± 6.87	20.77 ± 10.19	6.13 ± 1.88	409.37 ± 78.9	2382.98 ± 1279.78
p-value	0.267	0.711	*<0.001*	*<0.001*	0.006	6.53	*<0.001*	0.434

Note: Class 0: no stenoses/occlusions, class 1: at least one stenosis/occlusion. *p*-values obtained applying the Mann Whitney U test. A *p*-value of 0.05 or lower was considered statistically significant.
Abbreviations: AUC, area under the curve; HWHM, half width at half maximum; PI, peak intensity; TOA, time of arrival; TTP, time to peak .

4 | DISCUSSION

This study sought to implement a hemodynamic assessment of the BTK arteries in PAD patients using 4D-CT. To this end, three primary aims were envisaged: (i) arterial segmentation, (ii) TAC fitting and (iii) hemodynamic parameter assessment and correlation with PAD. Previous studies have shown the potential of 4D imaging (MRI & CT) concerning the assessment of blood flow velocity,[15,17] slope[16] and TTP.[44] However, to date, no study has quantified multiple hemodynamic parameters and flow rate and correlated them with stenoses present in the BTK arteries. The current study assesses 292 BTK arteries, acquired from 4D-CT imaging.

With respect to the first envisaged aim, we proposed an automated arterial segmentation method, combining motion correction, vessel segmentation and extraction of the the hemodynamic active sub region. 280 Out of 298 arteries were successfully segmented. Failures were caused by delayed contrast propagation, highlighting the challenge of dynamically imaging BTK arteries due to patient-to-patient variations. Similar to the findings of Metz *et al.*[33] the groupwise approach for motion correction yielded more robust and consistent results compared to the pairwise approach. Extracting the hemodynamically active sub region, as opposed to using the complete segmentation, improved the signal-to-noise ratio which, in turn, allowed for TAC fitting in less enhanced arteries.

Regarding the second aim, a 2D spatio-temporal method based on bicubic B-splines was introduced to fit the TAC's. The robustness of our approach with respect to interphase delay and imaging noise was assessed using simulated data. Based on these results, the 2D method outperformed the more commonly performed 1D temporal method as it consistently generated smooth TAC's and was less prone to introduce a bias. This finding was also reported by Giacalone *et al.*[26] who examined the robustness of a deconvolution algorithm with spatio-temporal regularization in perfusion MRI. The TASs provide the radiologist with an intuitive and quantitative visualization whereas before, it

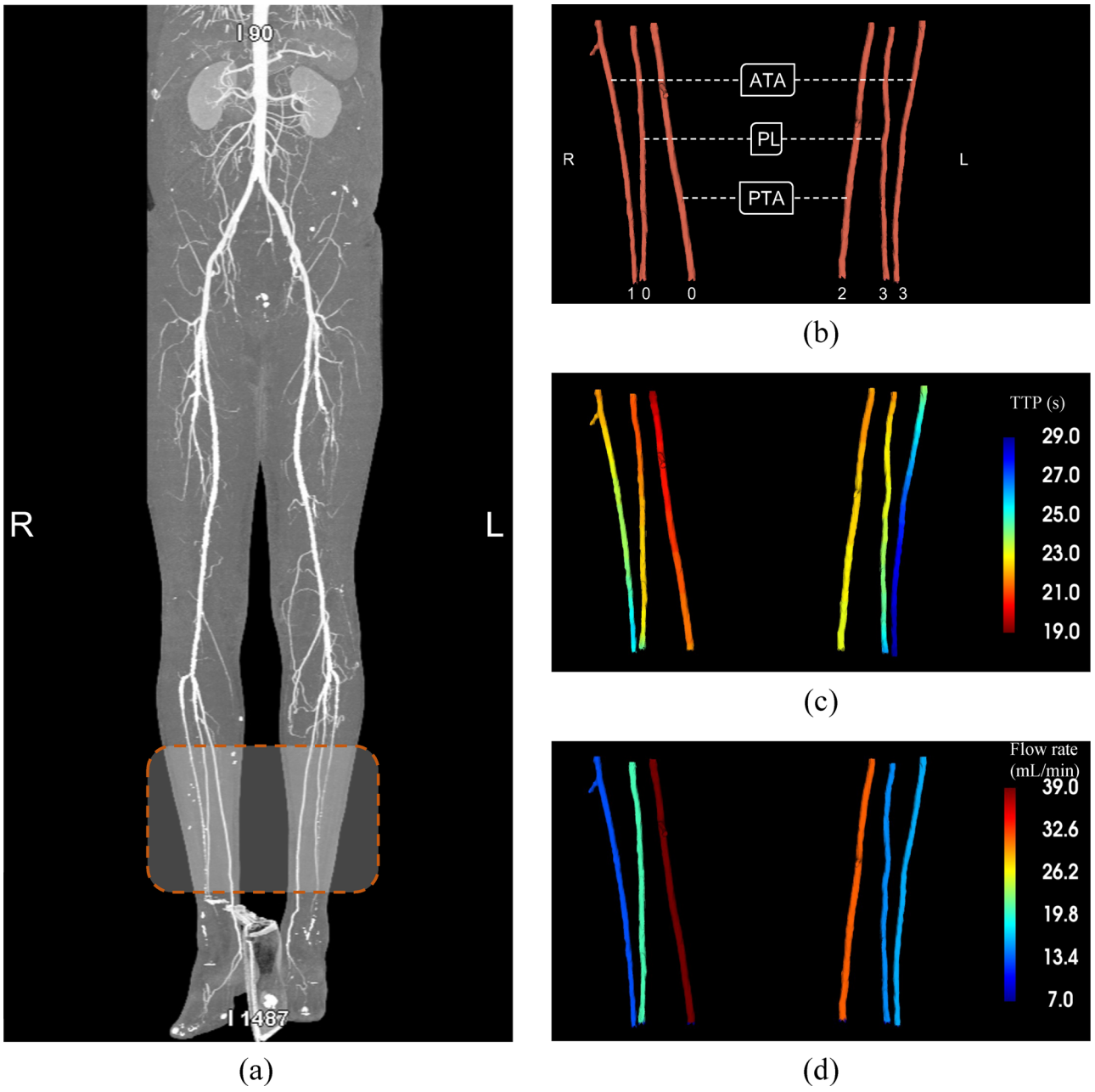

FIGURE 7 (a) MIP of the run-off CTA used as standard of care to display the vascular tree. The BTK arteries on both sides are opacified well but more distally, the arteries in the left calf and foot are less delineated. (b) Volume rendering of the segmentation of the BTK arteries. ATA, PL, PTA. (c) Volume rendering of the parametric map indicating the TTP (s) of each voxel by means of color-coding: early arrival of the contrast is depicted in red, late arrival in blue. (d) Volume rendering of the parametric map indicating the mean blood flow velocity (mm/s) by means of color-coding: low velocities are depicted in blue, high in red. ATA, anterior tibial artery; BTK, below-the-knee; CTA, computed tomography angiography; MIP, Maximum intensity projection; PL, peroneal artery; PTA, posterior tibial artery; TTP, time to peak.

could only be assessed separately in each arterial cross section and visualized in 2D.

As contemplated by the third aim of this study, we successfully derived hemodynamic parameters from the TAC's to characterize and quantify the arterial blood flow in the BTK arteries. Proximal stenoses were found to significantly hamper the blood flow, indicated by increased TOA and TTP values. In addition, the decreased slope and PI values demonstrate that proximal stenoses alter the shape of the TAC significantly by dispersing the contrast bolus. These findings are consistent with literature[16,45] as a non-obstructed flow will result in a sharp TAC, that is, large slope, high PI and small HWHM. The assessed mean blood flow velocities were within the range of characteristic blood flow velocities for stenotic and non-stenotic arteries (40–70 mm/s[46]). Additionally, the obtained flow rates are consistent with the literature.[47]

As expected, proximal stenoses caused a decrease in mean blood flow velocity. This decrease however was not significant. Blood flow velocity is susceptible to patient-to-patient variations and comparing velocities across patients without normalizing should therefore been done cautiously. Likewise, no significant difference in blood flow rate was found. Additionally, no significant differences between stenotic and non-stenotic arteries were found for the HWHM and AUC. The authors believe this is due to the incomplete TAC's in case of highly-stenotic arteries. The pseudo-clinical analysis of one patient illustrated that hemodynamic parameters not only support the results of the standard run-off CTA but are able to provide additional information which cannot be derived from standard run-off CTA. Firstly, the TTP rendering provides an intuitive and quantitative visualization of the differences in contrast arrival time between both legs. Secondly, the dominant artery could be selected based on the mean blood flow rate. This provides valuable information in order to devise an optimal angiosome-guided revascularisation strategy to ensure vascular inflow in the foot. The following limitations of our study merit consideration. Firstly, no normalization in terms of cardiac output, BMI, age or sex has been carried out at this point. Secondly, there was no ground truth available for the hemodynamic parameters and the accuracy of the hemodynamic parameter assessment could therefore not be determined. Current validation of the parameters was limited to studies on reproducibility and correlation with radiologically determined stenosis. Finally, using the proposed 4D-CT acquisition protocol (18 phases, $\Delta t = 2$s), we were unable to assess the complete TAC in heavily stenotic arteries. Based on the results of the reproducibility study in which data with larger interphase delay were simulated (nine phases, $\Delta t = 4$s) the total scan duration could potentially be increased while maintaining an equal patient radiation by increasing the interphase delay and applying spatio-temporal B-spline fitting for the TAC assessment. Further research might explore the advantage of a longer scan duration over a small interphase delay.

In conclusion, we proposed a segmentation method and a robust spatio-temporal B-spline regression for the automated assessment of hemodynamic parameters in stenotic BTK using 4D-CT imaging. Our study showcased the feasibility of extracting hemodynamic parameters using 4D-CT to describe and quantify the blood flow in the BTK arteries. Furthermore, our analysis revealed the potential of integrating dynamic CT scans into the PAD examination by correlating the hemodynamic parameters with the presence of proximal lesions. Among these parameters, the TOA, TTP, and PI emerged as particularly relevant from a clinical perspective.

ACKNOWLEDGMENTS

Pieter Thomas Boonen was funded by the Research Foundation Flanders (FWO), 1S63719N.

CONFLICT OF INTEREST STATEMENT

Tim Leiner grants or contracts from Dutch Technology Foundation, Netherlands Heart Foundation; royalties from Pie Medical; speakers bureau payments from Philips Healthcare, Bayer Healthcare; executive committee member and intermediate past president of the International Society for Magnetic Resonance in Medicine; shareholder, Quantib.

REFERENCES

1. Mascarenhas JV, Albayati MA, Shearman CP, Jude EB. Peripheral arterial disease. *Endocrinol Metab Clin North Am*. 2014;43:149-166.
2. Criqui MH, Aboyans V. Epidemiology of peripheral artery disease. *Circ Res*. 2015;116:1509-1526.
3. Fowkes FGR, Rudan D, Rudan I, et al. Comparison of global estimates of prevalence and risk factors for peripheral artery disease in 2000 and 2010: a systematic review and analysis. *Lancet*. 2013;382:1329-1340.
4. Joosten MM, Pai JK, Bertoia ML, et al. Associations between conventional cardiovascular risk factors and risk of peripheral artery disease in men. *JAMA, Tech Rep*. 2012;308(16):1660-1667.
5. Song P, Rudan D, Zhu Y, et al. Global, regional, and national prevalence and risk factors for peripheral artery disease in 2015: an updated systematic review and analysis. *Lancet Glob Health*. 2019;7:e1020-e1030.201.
6. Vlayen J, Kirsten HH, Olivier D, et al. Revascularization for lower limb peripheral arterial disease. *Good Clinical Practice (GCP) Brussels: Belgian Health Care Knowledge Centre (KCE)*. 2014. KCE Reports 221. D/2014/10/273/31.
7. Meyer BC, Oldenburg A, Frericks BB, et al. Quantitative and qualitative evaluation of the influence of different table feeds on visualization of peripheral arteries in CT angiography of aortoiliac and lower extremity arteries. *Eur Radiol*. 2008;18:1546-1555.
8. Foley WD, Stonely T. CT angiography of the lower extremities. *Radiol Clin North Am*. 2010;54(1):115-130.
9. Jens S, Koelemay MJ, Reekers JA, Bipat S. Diagnostic performance of computed tomography angiography and contrast-enhanced magnetic resonance angiography in patients with critical limb ischaemia and intermittent claudication: systematic review and meta-analysis. *Eur Radiol*. 2013;23:3104-3114.
10. Soulez G, Therasse E, Giroux M-F, et al. Management of peripheral arterial disease: role of computed tomography angiography and magnetic resonance angiography. *La Presse Méd*. 2011;40:e437-e452.
11. Leiner T, Carr JC. Noninvasive angiography of peripheral arteries. In: Hodler J, Kubik-Huch RA, von Schulthess GK, eds. *Diseases of the Chest, Breast, Heart and Vessels 2019-2022: Diagnostic and Interventional Imaging*. Springer; 2019:223-238.
12. Riffel P, Haubenreisser H, Higashigaito K, et al. Combined static and dynamic computed tomography angiography of peripheral artery occlusive disease: comparison with magnetic resonance angiography. *Cardiovasc Intervent Radiol*. 2018;41:1205-1213.
13. Prince MR, Chabra SG, Watts R, et al. Contrast material travel times in patients undergoing peripheral MR angiography. *Radiology*. 2002;224:55-61.
14. Ouwendijk R, Kock MC, Van Dijk LC, Van Sambeek MR, Stijnen T, Hunink MG. Vessel wall calcifications at multi-detector row CT angiography in patients with peripheral arterial disease: effect on clinical utility and clinical predictors. *Radiology*. 2006;241:603-608.
15. Harloff A, Zech T, Wegent F, Strecker C, Weiller C, Markl M. Comparison of blood flow velocity quantification by 4D flow MR imaging with ultrasound at the carotid bifurcation. *Am J Neuroradiol*. 2013;34(7):1407-1413.

16. Bovenschulte H, Krug B, Schneider T, et al. CT coronary angiography: coronary CT-flow quantification supplements morphological stenosis analysis. *Eur J Radiol*. 2013;82:608-616.
17. Markl M, Wallis W, Brendecke S, Simon J, Frydrychowicz A, Harloff A. Estimation of global aortic pulse wave velocity by flow-sensitive 4D MRI. *Magn Reson Med*. 2010;63(6):1575-1582.
18. Barfett JJ, Velauthapillai N, Fierstra J, et al. Intra-vascular blood velocity and volumetric flow rate calculated from dynamic 4D CT angiography using a time of flight technique. *Int J Cardiovasc Imaging*. 2014;30:1383-1392.
19. Sommer WH, Helck A, Bamberg F, et al. Diagnostic value of time-resolved CT angiography for the lower leg. *Eur Radiol*. 2010;20:2876-2881.
20. Buls N, de Brucker Y, Aerden D, et al. Improving the diagnosis of peripheral arterial disease in below-the-knee arteries by adding time-resolved CT scan series to conventional run-off CT angiography. First experience with a 256-slice CT scanner. *Eur J Radiol*. 2019;110:136-141.
21. Cuenod CA, Balvay D. Perfusion and vascular permeability: basic concepts and measurement in DCE-CT and DCE-MRI. *Diagn Interv Imaging*. 2013;94(12):1187-1204.
22. Cheong LH, Koh TS, Hou Z. An automatic approach for estimating bolus arrival time in dynamic contrast MRI using piecewise continuous regression models. *Phys Med Biol, Tech Rep*. 2003;48(5):N83.
23. Bennink E, Riordan AJ, Horsch AD, Dankbaar JW, Velthuis BK, De Jong HW. A fast nonlinear regression method for estimating permeability in CT perfusion imaging. *J Cereb Blood Flow Metab*. 2013;33:1743-1751.
24. Kasasbeh AS, Christensen S, Straka M, et al. Optimal computed tomographic perfusion scan duration for assessment of acute stroke lesion volumes. *Stroke*. 2016;47:2966-2971.
25. Peerlings D, Bennink E, Dankbaar JW, Velthuis BK, De Jong HWAM. Variation in arterial input function in a large multicenter computed tomography perfusion study On behalf of the DUtch acute STroke (DUST) study investigators. *Eur Radiol*. 2021;31(11):8317-8325.
26. Giacalone M, Frindel C, Robini M, Cervenansky F, Grenier E, Rousseau D. Robustness of spatio-temporal regularization in perfusion MRI deconvolution: an application to acute ischemic stroke. *Magn Reson Med*. 2017;78:1981-1990.
27. Bendinger AL, Debus C, Glowa C, Karger CP, Peter J, Storath M. Bolus arrival time estimation in dynamic contrast-enhanced magnetic resonance imaging of small animals based on spline models. *Phys Med Biol*. 2019;64(4):045003.
28. Chakwizira A, Ahlgren A, Knutsson L, Wirestam R. Non-parametric deconvolution using Bézier curves for quantification of cerebral perfusion in dynamic susceptibility contrast MRI. *Magn Reson Mater Phys Biol Med*. 2022;35(5):791-804.
29. Boonen PT, Buls N, Vandemeulebroucke J, et al. Quantification of blood velocity from time-resolved CT angiography on a 256-slice CT. In: Marti-Bonmati L, ed. *ECR 2018 - Book of Abstracts*. Springer Berlin Heidelberg; 2018:406-406.
30. The 2007 Recommendations of the International Commission on Radiological Protection. 2007;37(2-4),1-332.
31. McCormick M, Liu X, Jomier J, Marion C, Ibanez L. ITK: enabling reproducible research and open science. *Front Neuroinform*. 2014;8:13.
32. Polfliet M, Klein S, Huizinga W, Paulides MM, Niessen WJ, Vandemeulebroucke J. Intrasubject multimodal groupwise registration with the conditional template entropy. *Med Image Anal*. 2018;46:15-25.
33. Metz CT, Klein S, Schaap M, van Walsum T, Niessen WJ. Nonrigid registration of dynamic medical imaging data using nD+t B-splines and a groupwise optimization approach. *Med Image Anal*. 2011;15:238-249.
34. Farnebäck G, Westin CF. Improving Deriche-style recursive Gaussian filters. *J Math Imaging Vision*. 2006;26:293-299.
35. Antiga L, Steinman DA. *An image-based modeling framework for patient-specific computational hemodynamics.* Medical & biological engineering & computing; 2008;46(11):1097-1112.
36. Frangi AF, Niessen WJ, Vincken KL, Viergever MA. Multiscale vessel enhancement filtering. In: Wells WM, Colchester A, Delp S, eds. *Medical Image Computing and Computer-Assisted Intervention - MICCAI'98*. Springer Berlin Heidelberg; 1998:130-137.
37. Poiseuille JLM. Recherches sur la force du coeur aortique. *Didot*. 1828.
38. Unser M, Aldroubi A, Eden M. Fast B-spline transforms for continuous image representation and interpolation. *IEEE Trans Pattern Anal Mach Intell*. 1991;13:277-285.
39. Virtanen P, Gommers R, Oliphant TE, et al. SciPy 1.0: fundamental algorithms for scientific computing in Python. *Nat Methods*. 2020;17:261-272.
40. Calamante F. Arterial input function in perfusion MRI: a comprehensive review. *Prog Nucl Magn Reson Spectrosc*. 2013;74:1-32.
41. Riederer SJ, Haider CR, Borisch EA. Time-of-arrival mapping at three-dimensional time-resolved contrast-enhanced MR angiography. *Radiology*. 2009;253:532-542.
42. Pedregosa F, Michel V, Grisel O, et al. Scikit-learn: machine learning in python. *J Mach Learn Res, Tech Rep*. 2011;12:2825-2830.
43. Sommer WH, Helck A, Bamberg F, et al. Diagnostic value of time-resolved CT angiography for the lower leg. *Eur Radiol*. 2010;20:2876-2881.
44. Barfett JJ, Velauthapillai N, Fierstra J, et al. Intra-vascular blood velocity and volumetric flow rate calculated from dynamic 4D CT angiography using a time of flight technique. *Int J Cardiovasc Imaging*. 2014;30:1383-1392.
45. Lin CJ, Chang FC, Guo WY, et al. Changes of time-attenuation curve blood flow parameters in patients with and without carotid stenosis. *Am J Neuroradiol*. 2015;36:1176-1181.
46. Fronek A, Coel M, Berstein EF. Quantitative ultrasonographic studies of lower extremity flow velocities in health and disease. *Circulation*. 1976;53:957-960.
47. Osada T. Physiological aspects of the determination of comprehensive arterial inflows in the lower abdomen assessed by Doppler ultrasound. *Cardiovasc Ultrasound*. 2012;10:13.

How to cite this article: Boonen PT, Buls N, van Gompel G, et al. Quantitative hemodynamic assessment of stenotic below-the-knee arteries using spatio-temporal bolus tracking on 4D-CT angiography. *Med Phys*. 2023;50:6844–6856. https://doi.org/10.1002/mp.16755